Distinct Electrochemical Behavior of P3 and P2 Polytypes of Mn/Ni-based Na-ion Battery Cathode

Neha Dagar[1], Samriddhi Saxena[1], Hari Narayanan Vasavan[1], Asish Kumar Das[1], Pratiksha Gami[1], Sonia Deswal[2], Pradeep Kumar[2], Sunil Kumar[1,*]

[1]Department of Metallurgical Engineering and Materials Science, Indian Institute of Technology Indore, Simrol, 453552, India

[2]School of Physical Sciences, Indian Institute of Technology Mandi, Mandi, 175005, India

Corresponding author: sunil@iiti.ac.in, Tel: +91-7324-3063281

Abstract

A layered sodium-ion battery cathode $Na_{\frac{3}{4}}Mn_{\frac{11}{16}}Ni_{\frac{3}{16}}Al_{\frac{2}{16}}O_2$ (NMNA) prepared in P3 and P2 polytype structures by varying the calcination temperature is systematically investigated for its structural and electrochemical behavior. P3-phase prepared at 650 °C delivered a higher initial capacity of 164 mAh/g (~148 mAh/g for P2-phase calcined at 850 °C) at 0.1C. In contrast, the P2-phase sample exhibited better rate performance (87 mAh/g *vs.* 70 mAh/g for P3-phase at 4C) and capacity retention of ~47% after 200 cycles (only ~26% for P3-phase). Electrochemical impedance measurements before and after cycling confirmed that the increase in charge transfer resistance is responsible for the poor rate performance of the P3 phase.

Keywords: Sol-gel preparation; X-ray techniques; Electrical properties; Energy storage and conversion.

1. Introduction

The abundance and accessibility of Na resources have shifted the focus on Na-ion batteries as the potential replacement and complementary technology for grid storage and mobility applications. The development of Na-based layered oxide (Na_xTMO_2: TM is one or more redox–active 3d transition metals and other electrochemically inactive elements) cathodes with superior electrochemical characteristics is crucial for the wider commercialization of Na-ion batteries [1]. Na_xTMO_2 is classified into two distinct structural categories depending on the prismatic environment (P2, P3-type; x<0.85) and octahedral coordination (O3-type) for Na; 2 and 3 represent the numbers of transition metal layers in one unit cell [2-5]. The prismatic sites for Na allow facile Na-ion conductions and, therefore, better rate performance in P2 and P3 type phases, though these phases usually have lesser specific capacity than the O3-phase (x>0.85). Conversely, O3-type phases suffer from slow Na^+ diffusion kinetic and

typically lack satisfactory reversibility beyond 4.0 V due to an O3-to-P3 phase transformation but show high specific capacities [6-8].

Recently, there has been considerable focus on exploring the P3-phase as the cathode due to its lower synthesis temperature, smaller average particle size, and faster Na^+ diffusion. P3-phases have also enhanced the electrochemical behavior in P2/P3 biphasic cathodes [9, 10]. While having similar prismatic coordination for Na-ions, the P3 and P2 phases differ in the nature of phase transformations during (de)sodiation. P3 phases typically transform to the O3 phase through the sliding of TMO_2 layers. This transformation involves large volume change and degraded cyclability of the P3 cathode [11]. P2-type phases, on the other hand, are known to transform reversibly into P'2 and OP4 phases during sodium intercalation/deintercalation [1, 7, 9, 12]. In this work, the distinct electrochemical behavior of the P2 and P3 phases with the same chemical composition ($Na_{0.75}Mn_{0.6875}Ni_{0.1875}Al_{0.125}O_2$, NMNA) and the mechanisms responsible are discussed.

2. Experimental procedure

$Na_{0.75}Mn_{0.6875}Ni_{0.1875}Al_{0.125}O_2$ (NMNA) powders were prepared using a sol-gel method. The final calcination of the sample was carried out at 650 °C for 12 h (NMNA-P3 sample) and 850 °C for 12 h (NMNA-P2 sample) in air. The details of synthesis and structural and electrochemical characterization are provided in Supplementary Information.

3. Results and discussion

The XRD powder patterns of the NMNA samples calcined at 650 °C and 850 °C, along with Rietveld refinement profiles, are shown in Fig. 1(a) & (b) and confirm that NMNA-P3 adopts P3 stacking (space group: *R*3*m*) and NMNA-P2 crystallizes in space group $P6_3/mmc$ (Fig. 1c). No other peaks are discernable, confirming the monophasic nature of both samples. The calculated lattice parameters are $a=b=2.8720(2)$ Å, $c=16.755(2)$ Å and $V=119.69(2)$ Å^3 for P3-phase, and $a=b=2.8725(6)$ Å, $c=11.1913(5)$ Å and $V=79.976(5)$ Å^3 for P2-phase sample. Detailed structural parameters are summarized in Tables S1-S3 (Supplementary Material).

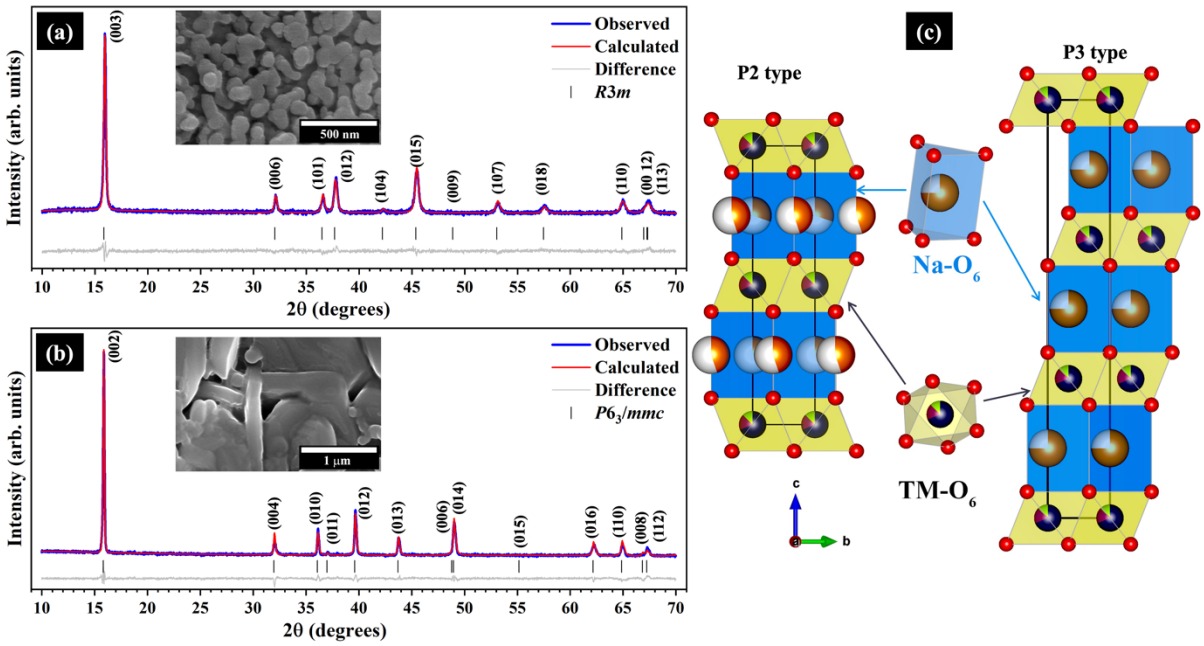

Fig. 1. Rietveld refinement profiles of the room temperature XRD data of (a) NMNA-P3 and (b) NMNA-P2. (c) Schematic illustrations of P3 and P2 type structures. FESEM images of NMNA-P3 and NMNA-P2 are given in (a) inset and (b) inset, respectively.

The morphologies of as-prepared NMNA samples were investigated by SEM. As shown in Fig. 1(b) inset, the particles for the P3-phase are spheroids with a much smaller average size (~130 nm) than the NMNA-P2 sample (~1 μm). A fair bit of particle agglomeration is apparent for the NMNA-P2 sample. The higher average particle size for P2 phases is attributed to the particle growth at higher calcination temperatures.

X-ray photoelectron spectra for various elements of both samples (Fig. 2) show fitted peaks corresponding to the binding energy of Ni^{2+} (Ni $2p_{1/2}$ and Ni $2p_{3/2}$ at 872.0 and 854.5 eV, respectively). Mn $2p$ spectrum is fitted with contributions from Mn^{3+} (Mn $2p_{3/2}$ peak at 642.35 eV) and Mn^{4+} (Mn $2p_{3/2}$ peak at 641.07 eV). The fitted XPS data confirms the presence of Mn^{3+}/Mn^{4+} states in the expected ratio ($Mn^{+3}_{0.25}Mn^{+4}_{0.4375}$). Similar spectra for NMNA-P3 and NMNA-P3 suggest that calcination temperature has no significant impact on the oxidation states of the electrochemically active Mn and Ni-ions.

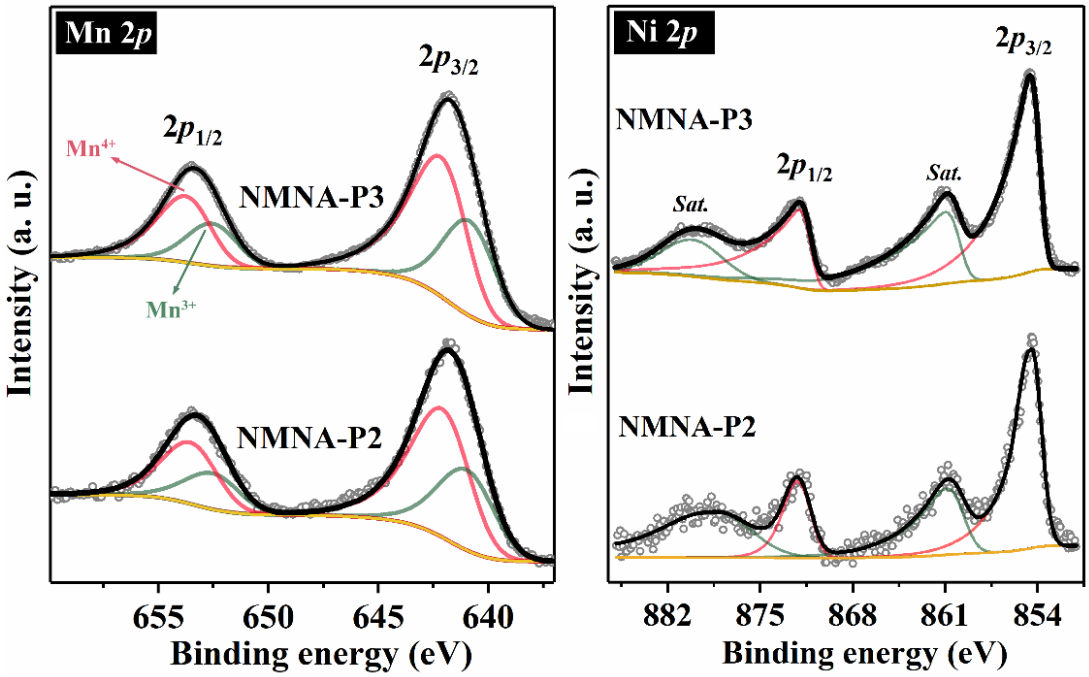

Fig. 2. X-ray photoelectron spectra of Mn 2*p* and Ni 2*p* for NMNA-P2 and NMNA-P3.

The galvanostatic charge-discharge performance of NMNA-P3 and NMNA-P2 cathodes in a voltage range of 1.5-4.4 V is shown in Fig. 3. The cells were cycled in wide voltage window to study the impact of $Mn^{3+/4+}$ activation and high-voltage phase transformation on the cyclability of these cathodes. The specific capacity of NMNA is assumed to be 160 mAh/g for C-rate calculation. At 0.1C, the discharge specific capacities of NMNA-P3 and NMNA-P2 are ~164 mAh/g and ~148 mAh/g, respectively (Fig. 3a). The differential capacity versus voltage (dQ/dV vs. V) plots reveal reversible redox couples with broad oxidation peaks at 2.29 V, 3.62/3.74V, and 4.20 V. The peaks below 2.5 V correspond to the Jahn-Teller active $Mn^{3+/4+}$ redox process, and peaks at ~3.7 V are due to the $Ni^{2+/4+}$ activity in both samples. The peak above 4 V is partially reversible (Fig. S1), is absent at higher C-rate, and is likely to arise from the anionic redox process [13].

The rate performance is given in Fig. 3b, and interestingly, the NMNA-P2 cathode performs better than the NMNA-P3 despite having a bigger average particle size. The discharge capacity decreases from 164 mAh/g at 0.1C to ~51 mAh/g at 4C for NMNA-P3. P2-type cathode shows excellent capacity of ~87 mAh/g even at 4C. Figure 3e shows the cycling behavior with a normalized capacity of NMNA-P3 and NMNA-P2 cathodes at 1C. The initial discharge capacities are ~85 mAh/g for NNNA-P3 and ~100 mAh/g for NMNA-P2. A considerable capacity deterioration upon prolonged cycling is observed in both cathodes with capacity retention of ~41% for NMNA-P2 and ~26% for NMNA-P3 phase after 200 cycles.

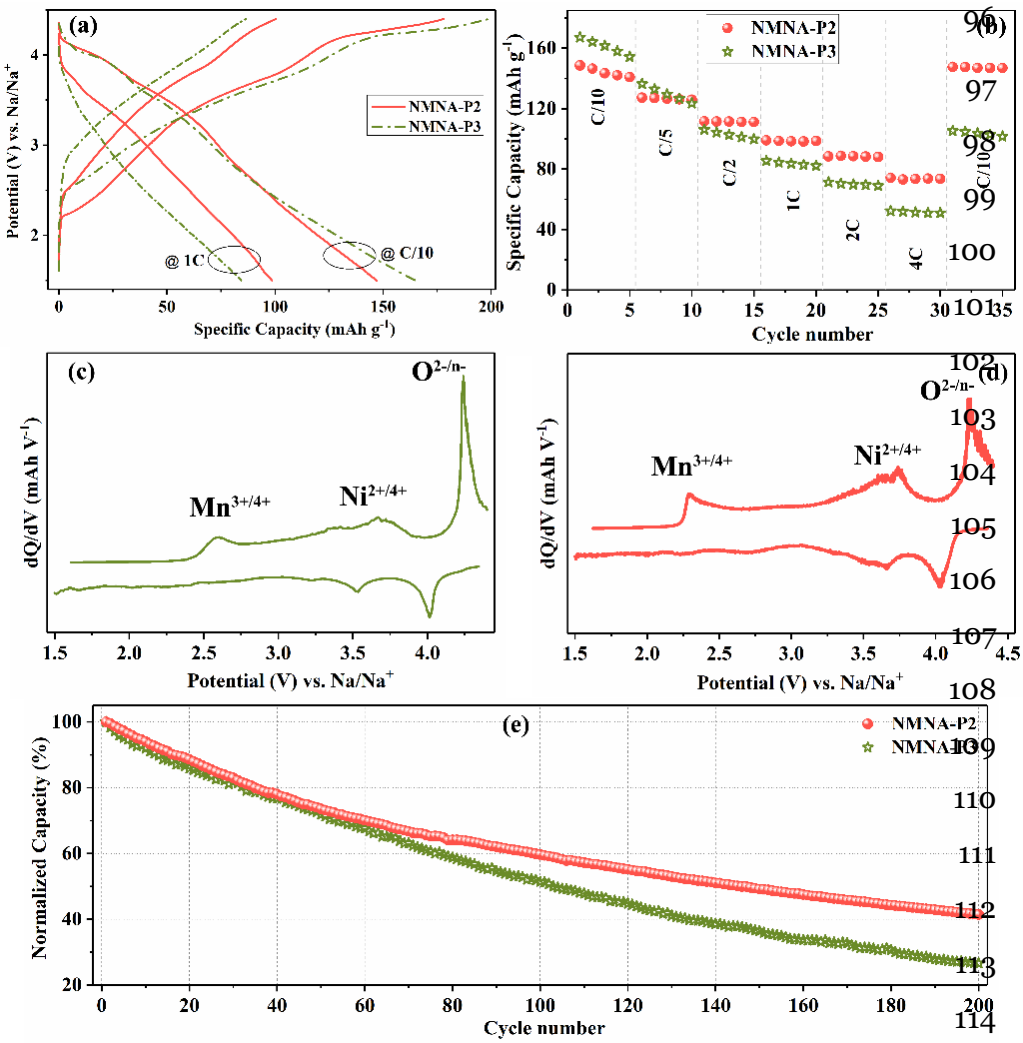

Fig. 3. (a) Galvanostatic-charge discharge voltage profiles of NMNA-P2 and NMNA-P3 cathodes at 0.1C and 1C in the voltage 1.5–4.4 V. (b) Rate-capability at current rates of 0.1C–5C, dQ/dV vs. V plots of NMNA-3 (c) and NMNA-P2 (d). (e) Long-term cycling stability at 1C.

To understand the reason behind the superior cyclability of the P2 phase, EIS measurements were conducted at various stages of charge on both NMNA-P3 & -P2 cells (before and after 200 charge/discharge cycles) by applying a 10 mV signal in the 100 kHz to 10 mHz frequency range. Nyquist plots of both cells are composed of overlapped semi-circular arcs in the high-frequency region and a straight in the low-frequency region (Fig. 4). The high-frequency intercept of the semi-circular arc indicates the electrolyte resistance (R_E), whereas arcs represent the resistance of the passivation layers formed on electrode surfaces (R_{PL}) and charge-transfer resistance (R_{CT}) [14]. The tail at low frequency represents the impedance associated with the ion diffusion in cathodes. The equivalent circuit (Fig. 4a2 inset) fitted EIS results indicate that, before cycling, the total resistance of the NMNA-P3 cell is lower than that of NMNA-P2 at 1.5 V (discharged state: 546 vs. 854 Ω) and 4.4 V (130 vs. 188 Ω), R_E remains constant (~5 Ω), and both R_{PL} & R_{CT} decrease with the increase in the state of

charge for both cells (Fig. 4(a1-a2) and 4(b1-b2)). After 200 charge-discharge cycles, the total resistance of both cells increases, and the increase is ~22.3% for P2 and ~232% for P3-phase (both measured at 4.4 V). Further, Nyquist plots in Fig. 4(b3-b4) show that the semicircular arc corresponding to the charge-transfer process becomes prominent for cycled NMNA-P3 cell. At 4.4 V, R_{CT} increased from 22 Ω (Fig. 4(b2)) to 286 Ω after 200 cycles (Fig. 4(b4)); the change in R_{PL} is comparatively smaller, from 103 to 140 Ω.

Fig. 4. Room temperature Nyquist plots for cells at charged (4.4 V) and discharged state (1.5 V): NMNA-P2 cell before (a1-a2) and after 200 cycles (a3-a4) and (b) NMNA-P3 cell before (b1-b2) and

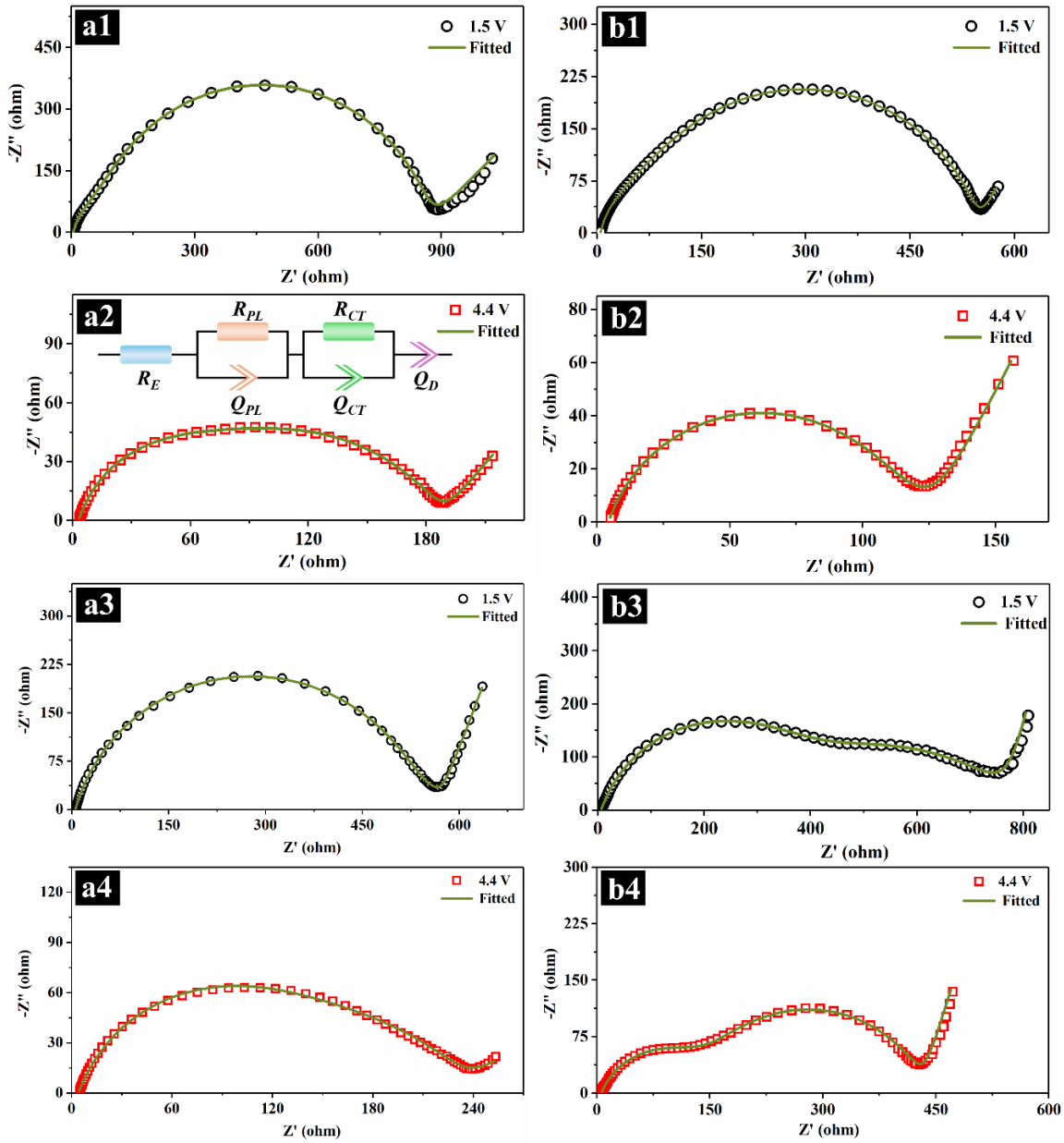

after 200 cycles (b3-b4).

In contrast to other reports, the P3 phase in this study (despite smaller average particle size) showed poor rate performance as compared to the P2 phase when cycled in the 1.5–4.4 V

range. Slow charge transfer kinetics of the P3 phase, as confirmed by the EIS experiments, are responsible for the poor rate performance. Besides, the capacity decay suggested that cycling in 1.5–4.4 V is much more detrimental to P3 phase stability than the P2 phase. While Jahn-Teller distortion due to $Mn^{3+/4+}$ redox activation below 2.5 V is expected in both samples, the P3↔O3 phase transformations induced particle cracking & exfoliation and smaller particle size (larger surface passivation layer) could be responsible for poor rate performance and inferior cycle stability of NMNA-P3 sample [11]. Protective coating on the particle surface, mixed-phase structure, etc., should be explored to circumvent such issues.

4. Conclusion

In this study, a novel Mn/Ni-based composition ($Na_{\frac{3}{4}}Mn_{\frac{11}{16}}Ni_{\frac{3}{16}}Al_{\frac{2}{16}}O_2$) was synthesized. Its electrochemical behavior was strongly dependent on crystal structure. The NMNA-P2 cathode exhibited superior rate performance (87 mAh/g at 4C) and cyclability, while the NMNA-P3 provided higher initial specific capacity at 0.1C rate (164 mAh/g). EIS measurements on cycled cells confirmed a much larger increase in charge-transfer and electrode passivation layer resistance in the P3 cathode, which explains the much inferior rate performance of the NMNA-P3 cathode.

Acknowledgment

SK thanks the Science and Engineering Research Board (SERB), Government of India, for the financial support (grant number: CRG/2021/005548).

References

[1] N. Yabuuchi, K. Kubota, M. Dahbi, S. Komaba, Chem. Rev., 114 (2014) 11636-11682.
[2] C. Delmas, C. Fouassier, P. Hagenmuller, Physica B+C, 99 (1980) 81-85.
[3] Y. Zhang, J. Chen, R. Wang, L. Wu, W. Song, S. Cao, Y. Shen, X. Zhang, X. Wang, ACS Appl. Mater. Interfaces, 16 (2024) 11349-11360.
[4] K. Tang, Y. Huang, X. Xie, S. Cao, L. Liu, H. Liu, Z. Luo, Y. Wang, B. Chang, H. Shu, X. Wang, Chem. Eng. J., 399 (2020) 125725.
[5] K. Tang, Y. Huang, X. Xie, S. Cao, L. Liu, M. Liu, Y. Huang, B. Chang, Z. Luo, X. Wang, Chem. Eng. J., 384 (2020) 123234.
[6] M. Sathiya, Q. Jacquet, M.L. Doublet, O.M. Karakulina, J. Hadermann, J.M. Tarascon, Adv. Energy Mater., 8 (2018) 1702599.
[7] R.J. Clément, P.G. Bruce, C.P. Grey, J. Electrochem. Soc., 162 (2015) A2589.
[8] S. Saxena, H.N. Vasavan, M. Badole, A.K. Das, S. Deswal, P. Kumar, S. Kumar, J. Energy Storage, 64 (2023) 107242.
[9] H.N. Vasavan, M. Badole, S. Saxena, V. Srihari, A.K. Das, P. Gami, S. Deswal, P.

Kumar, S. Kumar, Mater. Today Energy, 37 (2023) 101380.

[10] Y.-N. Zhou, P.-F. Wang, Y.-B. Niu, Q. Li, X. Yu, Y.-X. Yin, S. Xu, Y.-G. Guo, Nano Energy, 55 (2019) 143-150.

[11] T. Risthaus, L. Chen, J. Wang, J. Li, D. Zhou, L. Zhang, D. Ning, X. Cao, X. Zhang, G. Schumacher, M. Winter, E. Paillard, J. Li, Chem. Mater., 31 (2019) 5376-5383.

[12] N. Nair, S.V. Nair, S. Baskar, Mater. Lett., 354 (2024) 135397.

[13] B. Chen, Y. Xin, Y. Wang, X. Ding, C. Jiang, F. Wu, H. Gao, Energy Storage Mater., 67 (2024) 103252.

[14] T.P. Heins, N. Harms, L.-S. Schramm, U. Schröder, Energy Tech., 4 (2016) 1509-1513.

[Supplementary Material]

Distinct Electrochemical Behavior of P3 and P2 Polytypes of Mn/Ni-based Na-ion Battery Cathode

Neha Dagar[1], Samriddhi Saxena[1], Hari Narayanan Vasavan[1], Asish Kumar Das[1], Pratiksha Gami[1], Sonia Deswal[2], Pradeep Kumar[2], Sunil Kumar[1,*]

[1]Department of Metallurgical Engineering and Materials Science, Indian Institute of Technology Indore, Simrol, 453552, India

[2]School of Physical Sciences, Indian Institute of Technology Mandi, Mandi, 175005, India

**Corresponding author: sunil@iiti.ac.in, Tel: +91-7324-3063281*

Synthesis and characterization

$Na_{0.75}Mn_{0.6875}Ni_{0.1875}Al_{0.125}O_2$ (NMNA) powders were prepared by sol-gel method using sodium nitrate, manganese nitrate, nickel nitrate, and aluminum nitrate as the starting precursors; citric acid was used the chelating agent. After dissolving these precursors in de-ionized water, the solution was stirred at 80 °C for 12 h. After grinding, the dried mixture was pre-calcined at 500 °C. Further, parts of this mixture were calcined at 650 °C for 12 h (labeled as NMNA-P3) and 850 °C for 12 h (labeled as NMNA-P2) in air to obtain the desired phases.

Powder X-ray diffraction (XRD) studies were carried out using a Panlytical diffractometer in the 2θ range of 10 – 70° at room temperature, and the Rietveld refinement of the XRD data was performed using the TOPAS software. A JEOL scanning electron microscope was used for microstructure analysis. X-ray photoelectron spectroscopy (XPS) measurements were conducted using a Thermofisher Scientific (Naxsa base) instrument equipped with a 1486.6 eV (Al Kα) X-ray source. Galvanostatic charge-discharge (GCD) and electrochemical impedance spectroscopy (EIS) measurements were performed using a Neware battery tester and NFCorp. LCR meter, respectively. CR2032-type half-cells for these measurements were fabricated using the slurry (NMNA-P2 powder, Ketjen black, and PVDF in 80:10:10 ratio) coated on an aluminum current collector as the working electrode and sodium metal as the counter electrode. 1M $NaClO_4$ in EC: PC (1: 1 vol.) was the electrolyte.

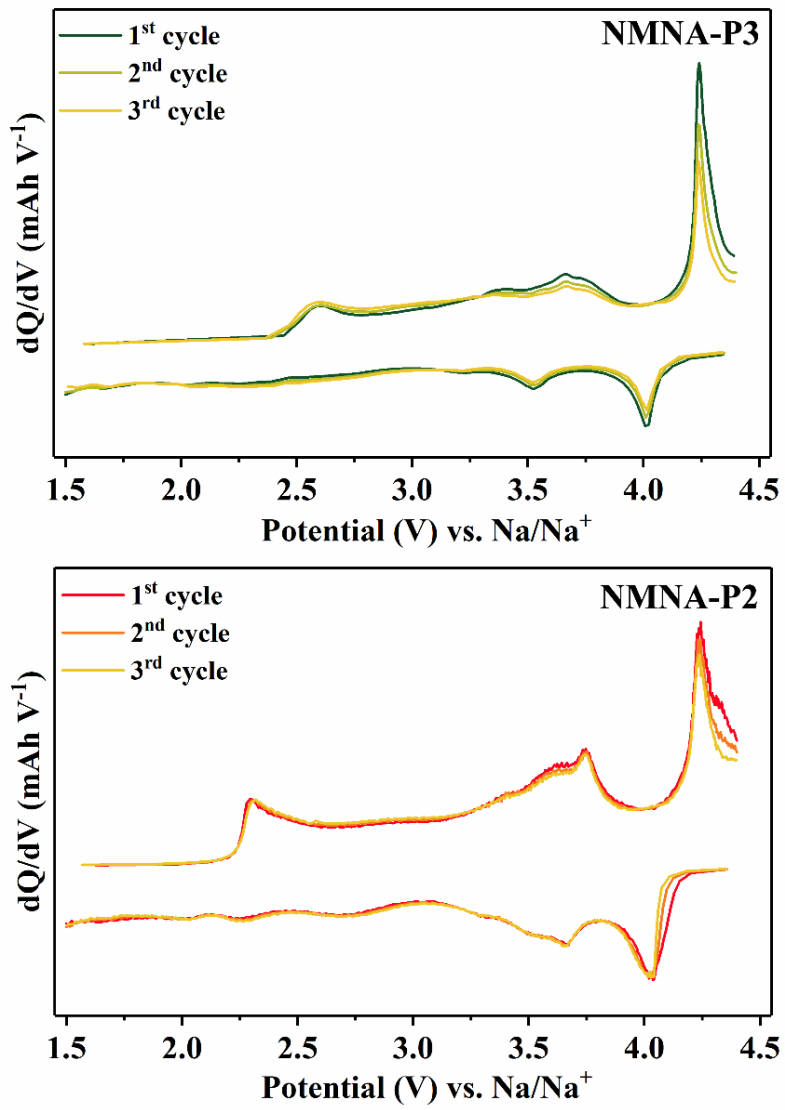

Figure S1: dQ/dV vs. V plots of NMNA-3 and NMNA-P2 cells for three cycles at 0.1C.

Table S1: Refined structural parameters for $Na_{\frac{3}{4}}Mn_{\frac{11}{16}}Ni_{\frac{3}{16}}Al_{\frac{2}{16}}O_2$ powder at 298 K.

Composition	$\mathbf{Na_{\frac{3}{4}}Mn_{\frac{11}{16}}Ni_{\frac{3}{16}}Al_{\frac{2}{16}}O_2}$	
Synthesis temperature	650 °C	850 °C
Type	P3	P2
Crystal system	Trigonal	Hexagonal
Space group	*R*3*m*	*P*6$_3$/*mmc*
Cell Parameters, Å		
	a = 2.8720(2)	*a* = 2.87258(6)
	c = 16.755(2)	*c* = 11.1913(5)
Cell Volume V, Å^3	119.69(2)	79.976(5)
Z	3	2
Phase density (g/cm^3)	~ 4.2197(9)	~ 4.2102(2)

Table S2: Results of Rietveld refinement of room temperature (298K) powder x-ray diffraction data for NMNA-P3 phase. *x*, *y*, *z* — positional coordinates. Reliability Factors: R_{EXP}, R_{WP}, R_P, and GoF were 2.06, 2.34, 1.84, and 1.14, respectively.

Atom	*Wyckoff position*	*x*	*y*	*z*	*Occupancy*
Na	3a	0	0	0.1672(5)	0.75
Mn/Ni/Al	3a	0	0	0	0.6875/0.1875/0.125
O1	3a	0	0	0.3963(3)	1
O2	3a	0	0	-0.3963(3)	1

Table S3: Results of Rietveld refinement of room temperature (298K) powder x-ray diffraction data for NMNA-P2 phase. *x*, *y*, *z* — positional coordinates. Reliability Factors: R_{EXP}, R_{WP}, R_P, and GoF were 2.05, 2.92, 2.12, and 1.42, respectively.

Atom	*Wyckoff position*	*x*	*y*	*z*	*Occupancy*
Na1	2b	0	0	1/4	0.297(3)
Na2	2d	2/3	1/3	1/4	0.452(3)
Mn/Ni/Al	2a	0	0	0	0.6875/0.1875/0.125
O	4f	2/3	1/3	0.0958(6)	1